ISSN 0031-918X, Physics of Metals and Metallography, 2017, Vol. 118, No. 6, pp. 601–607. © Pleiades Publishing, Ltd., 2017.
Original Russian Text © A.N. Petrova, I.G. Brodova, S.V. Razorenov, 2017, published in Fizika Metallov i Metallovedenie, 2017, Vol. 118, No. 6, pp. 632–638.

STRENGTH AND PLASTICITY

Strength Properties and Structure of a Submicrocrystalline Al–Mg–Mn Alloy under Shock Compression

A. N. Petrova[a, b, *], I. G. Brodova[a], and S. V. Razorenov[c, d]

[a] *Mikheev Institute of Metal Physics, Ural Branch, Russian Academy of Sciences, ul. S. Kovalevskoi 18, Ekaterinburg, 620137 Russia*

[b] *Yeltsin Ural Federal University, ul. Mira 19, Ekaterinburg, 620002 Russia*

[c] *Institute of Problems of Chemical Physics, pr. Semenova 1, Chernogolovka, Moscow region, 142432 Russia*

[d] *National Research Tomsk State University, pr. Lenina 36, Tomsk, 634050 Russia*

**e-mail: petrovanastya@yahoo.com*

Received October 18, 2016; in final form, December 15, 2016

Abstract—The results of studying the strength of a submicrocrystalline aluminum A5083 alloy (chemical composition was 4.4Mg–0.6Mn–0.11Si–0.23Fe–0.03Cr–0.02Cu–0.06Ti wt % and Al for balance) under shock-wave compression are presented. The submicrocrystalline structure of the alloy was produced in the process of dynamic channel-angular pressing at a rate of 10^4 s^{-1}. The average size of crystallites in the alloy was 180–460 nm. Hugoniot elastic limit σ_{HEL}, dynamic yield stress σ_y, and the spall strength σ_{SP} of the submicrocrystalline alloy were determined based on the free-surface velocity profiles of samples produced by shock compression. It has been established that upon shock compression the σ_{HEL} and σ_y of the submicrocrystalline alloy are higher than those of the coarse-grained alloy and σ_{sp} does not depend on the grain size. The maximum value of σ_{HEL} reached for the submicrocrystalline alloy is 0.66 GPa, which is greater than that in the coarse-crystalline alloy by 78%. The dynamic yield stress is $\sigma_y = 0.31$ GPa, which is higher than that of the coarse-crystalline alloy by 63%. The spall strength is $\sigma_{sp} = 1.49$ GPa. The evolution of the submicrocrystalline structure of the alloy was investigated during shock compression. It has been established that a mixed nonequilibrium grain-subgrain structure with a fragment size of about 400 nm is retained after shock compression, and the dislocation density and the hardness of the alloy are increased.

Keywords: dynamic strength, shock compression, submicrocrystalline structure

DOI: 10.1134/S0031918X17060072

INTRODUCTION

The main task of studying the high-strain-rate deformation processes and the fracture of metals and alloys is to predict the action of high-strain-rate impacts, explosions, or other pulsed actions on commercial metallic materials and products made from them. In recent years, submicrocrystalline (SMC) materials, including aluminum alloys, with high strength characteristics due to a decrease in the grain size as a result of severe plastic deformation, are proposed for high-duty constructions and their small-dimension components operating under extreme conditions. One of the directions of study in this area is the behavior of these materials under shock-wave loading; however, the amount of these data is quite insufficient and the results of these studies are frequently quite ambiguous [1–5]. Almost all SMC metals and investigated alloys do not display a significant increase in the strength characteristics under dynamic loading compared to static and quasi-static deformation conditions. Thus, the results of dynamic experiments with aluminum alloys [6, 7] have shown that a 100-fold decrease in the grain size produced by severe plastic deformation can lead to an increase in the Hugoniot elastic limit by a few dozen percents and that, under spall-fracture conditions, the tensile strength varies only slightly. However, the same parameters can also increase severalfold during static loading. It can be considered to be proved that the mechanical behavior of the SMC materials formed by severe plastic deformation is determined in quasi-static tests, not only by the grain size, but also strongly depends on the structural characteristics, such as the defect density, the ratio of the amounts of low and high-angle boundaries, the presence of second phases, and so on [8]. As was shown in [9, 10], the employment of dynamic channel-angular pressing (DCAP) for severe plastic deformation makes it possible to vary these character-

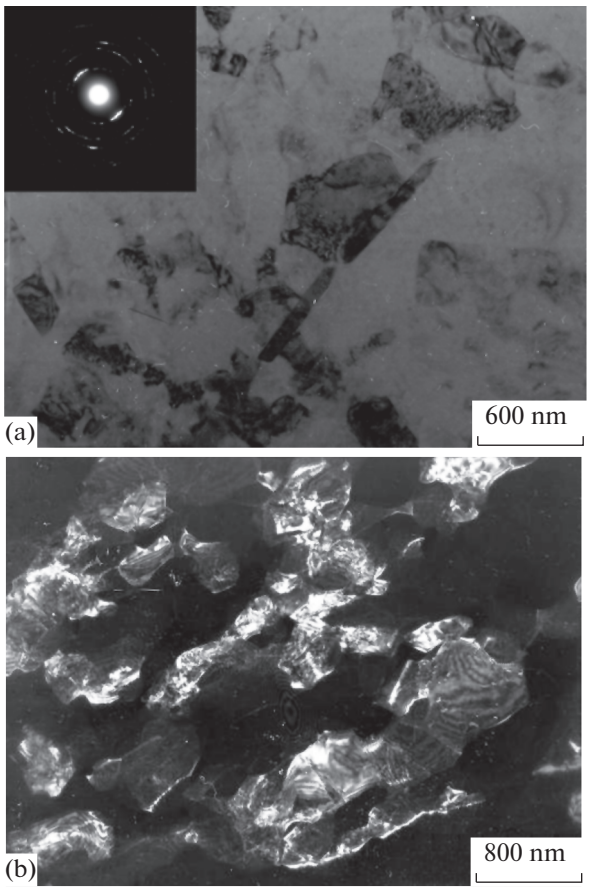

Fig. 1. Structure of A5083 alloy after double pressing at V = 250–300 m/s. TEM: (a) bright-field image and (b) dark-field image taken in the reflection g_{Al} = 111.

istics of the SMC aluminum alloys in a wide range. Among metals with an fcc lattice, aluminum and its alloys are distinguished by a high energy of stacking faults, a high mobility of dislocations, and a relatively low melting point; therefore, when using quasi-static methods of deformation, the main mechanisms of the formation of an SMC structure are the dynamic recovery and recrystallization [11–13]. At strain rates that are five to six orders of magnitude higher, these processes of the relaxation of elastic energy are not determinative in these alloys. In [9, 10], a clear dependence of the type of the SMC structure produced by DCAP on the mobility of a dislocation ensemble was established, i.e., on the degree of alloying of the matrix and on the presence of second phases, was established in [9, 10]. The behavior of materials with an SMC structure produced by DCAP under of shock-loading conditions differs from the behavior of SMC alloys produced by low-strain-rate plastic deformation, e.g., by equal-channel angular pressing (ECAP) [14, 15]. It has been established on the example of commercial aluminum and commercial aluminum alloys of grades AMts and B95 [14] that the SMC materials formed by DCAP retain high characteristics of elastic–plastic transition and dynamic strength at a strain rate of $\sim 10^5$ s^{-1}.

The purpose of this work was to continue studying the behavior of aluminum SMC alloys upon a shock-wave impact and the determination of the structural features and the resistance to dynamic deformation and fracture of an industrial Al–Mg–Mn alloy (A5083).

EXPERIMENTAL

In this work, we investigated the behavior of SMC and coarse-grained (CG) A5083 alloy with the chemical composition (wt %) 4.4Mg–0.6Mn–0.11Si–0.23Fe–0.03Cr–0.02Cu–0.06Ti and Al for balance. Dynamic channel-angular pressing was used to produce samples with an SMC structure. Cylindrical samples cut out of an extruded rod with a diameter of 14 mm and a length of 70 mm were loaded using the piston scheme of DCAP deformation [16]. The samples were deformed in the regime close to simple shear in an equipment with two intersecting channels at a rate of $\sim 10^4$ s^{-1} under the action of the energy of gunpowder gases. A repeated pressing cycle was carried out according to route B_c, when the sample is rotated through 90° about its axis counterclockwise between the cycles. The initial velocity (V) of the samples upon DCAP was 150 and 250–300 m/s, and the number of cycles of pressing was N = 1 and 2.

The features of the SMC structure formed in an A5083 alloy during DCAP were described in detail in [17]. The main distinguishing characteristics of the studied SMC states are the fragment sizes and the fraction of high-angle boundaries in the structure of the aluminum matrix. After one DCAP cycle, regardless of the speed-up, the structure represents shear microbands consisting of elongated and weakly misaligned fragments separated by low-angle boundaries. An increase in the sample speed from 150 to 300 m/s led to an increase in the average size of fragments from 180 to 240 nm and to an increase in the fraction of high-angle boundaries. The structural state of the alloy changes significantly during a repeated cycle (V = 250–300 m/s, N = 2). In this case, a mixed SMC structure is typical and characterized by the presence of fragments with low-angle boundaries and a large number of grains with a high-angle misorientations (Fig. 1). The average grain/subgrain size is 460 nm.

Dynamic pressing leads to a refinement of the matrix structure by five to seven times compared with the CG state, which in turn increases the yield stress and the ultimate tensile strength under static tension by 1.3–1.5 times [18].

In the case of shock-wave experiments, the CG samples and samples with an SMC structure in the form of disks with a diameter of ~14–20 mm and a thickness of ~2 mm were shock loaded by a flat aluminum plate with a thickness of ~0.4 mm, which was

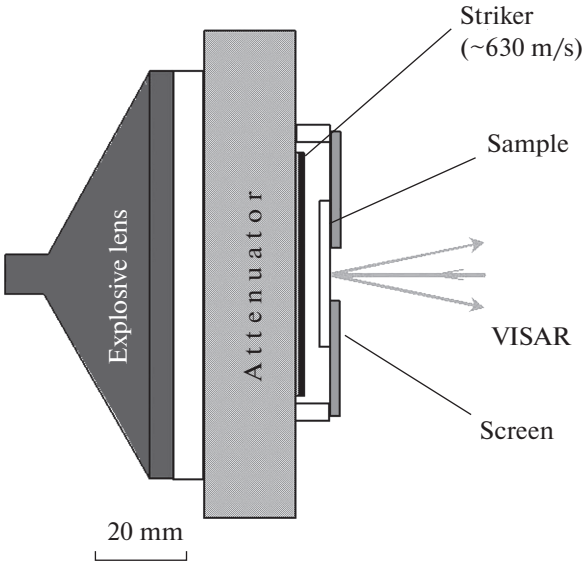

Fig. 2. Scheme of experiments on the shock-wave loading and registration of the free-surface velocity profiles of aluminum-alloy samples using a VISCAR laser interferometer.

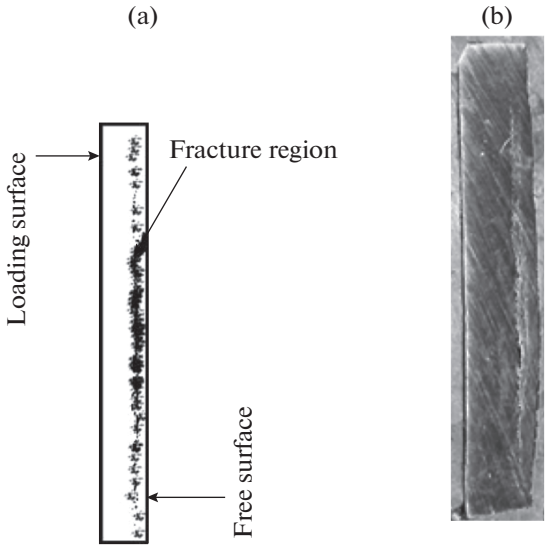

Fig. 3. (a) Schematic representation and (b) photograph of a retained sample in the cross section.

accelerated to 620 ± 30 m/s using an explosive device [19]. Under these conditions of collision, the maximum compression pressure was 4–5 GPa.

The scheme of wave-shock experiments is presented in Fig. 2. To determine the mechanical characteristics of the materials during loading, we recorded full free-surface velocity profiles $U_{fs}(t)$ (wave profiles) using a VISAR laser Doppler speed meter [20]. The ratio of the thicknesses of the striker and the sample allowed us to implement spall fracture conditions in the sample. The Hugoniot elastic limit σ_{HEL}, dynamic yield stress σ_y, spall strength σ_{sp}, and the thickness of the spall plate h_{sp} were determined from an analysis of the wave profiles.

When calculating the shock compression pressure of the samples, $P = \rho_0 W U_{fs}$, we used the Hugoniot adiabat of aluminum in the form $W = 5.35 + 1.34U_{fs}/2$ [21], where ρ_0 is the initial density of the material and W is the shock-wave velocity. To study the evolution of the SMC structure of the alloy under shock compression, special experiments at the retained samples were performed. To implement the conditions of spall fracture and the retention of a sample without any additional deformation, the sample was slowed down almost to a complete stop in a thick layer of fresh snow (about 1 m), which played the role of a soft environment with a very low dynamic impedance in these experiments. The schematic image of a retained sample with internal fracture in the cross section and a photo of a real retained sample are presented in Fig. 3.

The fine structure of retained SMC samples was investigated in three regions, namely, near the loading surface, in the fracture region, and at the free surface, using a Philips CM-30 transmission electron microscope (TEM) at an accelerating voltage of 200 kV. X-ray diffraction (XRD) analysis was carried out using a DRON-3M X-ray diffractometer in Cu $K\alpha$ radiation. Based on the X-ray diffraction patterns, we calculated the lattice parameter of the aluminum matrix (a), the mean-square microstrain of the crystal lattice ($\langle \varepsilon^2 \rangle^{1/2}$), and the coherent domain sizes (D_{rcscd}). The dislocation density was calculated by the formula $\rho_d = 2\sqrt{3}\langle \varepsilon^2 \rangle^{1/2} / (D_{cd} \times b)$, where $b = a\sqrt{2}/2$ is the Burgers vector for fcc metals. The microhardness HV was measured using a PMT-3 device at a load of 0.2 N (the error did not exceed 10%).

RESULTS AND DISCUSSION

Figure 4 displays the free-surface velocity profiles of all SMC and CG samples obtained upon shock compression. All wave profiles show typical features observed upon the spall fracture of aluminum alloys [2, 5, 14, 22]. The wave profiles demonstrate features that correspond to the emergence of an elastic precursor, of a plastic shock wave of compression, and of part of the following rarefaction wave onto the surface. The weak increase in the surface velocity in front of the elastic wave is due to the effect of an air-compression wave, which forms in front of the striker during its acceleration before the collision on the sample. At the selected ratio of the thickness of the striker and the sample (approximately 1 : 5), the conditions of loading near the free back surface of the sample correspond to the beginning of the attenuation of the shock wave under the action of the overtaking rarefaction wave; as

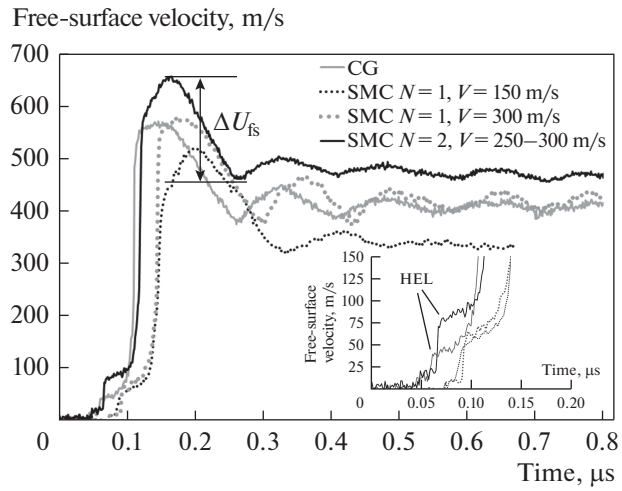

Fig. 4. Free-surface velocity profiles for SMC and CG samples of A5083 alloy obtained under shock compression.

a result, the compression pulse has approximately a triangular shape. When the compression pulse is reflected from the free surface of the sample, tensile stresses that lead to spall fracture are generated inside the sample. Upon the formation of a spall crack, the relaxation of tensile stresses occurs; as a result, a compression wave (spall pulse) forms and causes the second rise of the free-surface velocity when it reaches the surface. The damped velocity oscillations are associated with multiple reflections of a spall pulse in a separated plate. It should be noted that the variations in the maximum velocity (the maximum pressure of shock compression) in these experiments are connected with the scatter of the striker velocities, which could reach ±50 m/s in these experiments.

The Hugoniot elastic limit of the material is determined from the wave profiles as [22]

$$\sigma_{HEL} = \rho_0 C_L U_{fs}^{HEL}/2,$$

where C_L is the longitudinal sound velocity in the material and U_{fs}^{HEL} is the free-surface velocity behind the front of the elastic precursor.

The Hugoniot elastic limit corresponds to the conditions of uniaxial deformation; its conversion to the yield stress under the standard conditions of uniaxial stress state σ_y is made using the simple expression [22]

$$\sigma_y = \frac{3}{2}\sigma_{HEL}\left(1 - C_B^2/C_L^2\right),$$

where C_B is the bulk velocity of sound [22].

The decrement of the surface velocity ΔU_{fs} (Fig. 4) during the decrease in the velocity from the maximum to the value achieved in front of the spall pulse is proportional to the breaking stress, i.e., the spall strength of the material (σ_{sp}). In the linear (acoustic) approximation, the spall strength is calculated as [22]

$$\sigma_{sp} = 1/2\,\rho_0 C_B(\Delta U_{fs} + \delta U),$$

where δU is the correction for the distortion of the wave profile due to the difference between the front velocity of the spall pulse and the velocity of the plastic part of the incident rarefaction wave in front of it [22]. These distortions take place, since the spall-pulse front is an elastic compression wave in a stretched material and overtakes the unloading part of the incident compression pulse that move with the bulk velocity of sound. The thickness of the spall plate h_{sp} can be determined from the surface-velocity profiles $U_{fs}(t)$, from the period of oscillations of the velocity. Here, the fact that the wave front is repeatedly reflected inside the spall plate and moves with the longitudinal velocity of sound was taken into account; therefore, h_{sp} is determined from the period of velocity oscillation Δt as $h_{sp} = C_L \Delta t/2$.

The results of calculating the dynamic characteristics based on an analysis of the wave profiles and some constants of materials are given in Table 1, where ν is Poisson's ratio.

From this table, it can be seen that, under shock compression, all strength characteristics of SMC samples are higher than those of the CG analogs. Moreover, different structural SMC states, which depend on regime of the DCAP, affect the dynamic characteristics; in particular, when V ($N = 1$) increases, they increase; i.e., the Hugoniot elastic limit increases by 36% and the dynamic yield stress increases by 72%. The formation of the grain–subgrain structure (at $N =$

Table 1. Dynamics characteristics of the alloy in the SMC and CG states

Description	Material constants	σ_{HEL}, GPa	σ_y, GPa	σ_{sp}, GPa	h_{sp}, mm
CG	$C_L = 6.33$ km/s, $\nu = 0.33$, $H_V = 970$ MPa	0.37	0.19	1.52	0.45
SMC $N = 1$, $V = 150$ m/s	$C_L = 6.45$ km/s, $\nu = 0.36$, $H_V = 1150$ MPa	0.41	0.18	1.50	0.46
SMC $N = 1$, $V = 300$ m/s	$C_L = 6.457$ km/s, $\nu = 0.31$, $H_V = 1200$ MPa	0.56	0.31	1.50	0.42
SMC $N = 2$, $V = 250$ m/s	$C_L = 6.41$ km/s, $\nu = 0.345$, $H_V = 1200$ MPa	0.66	0.31	1.48	0.46

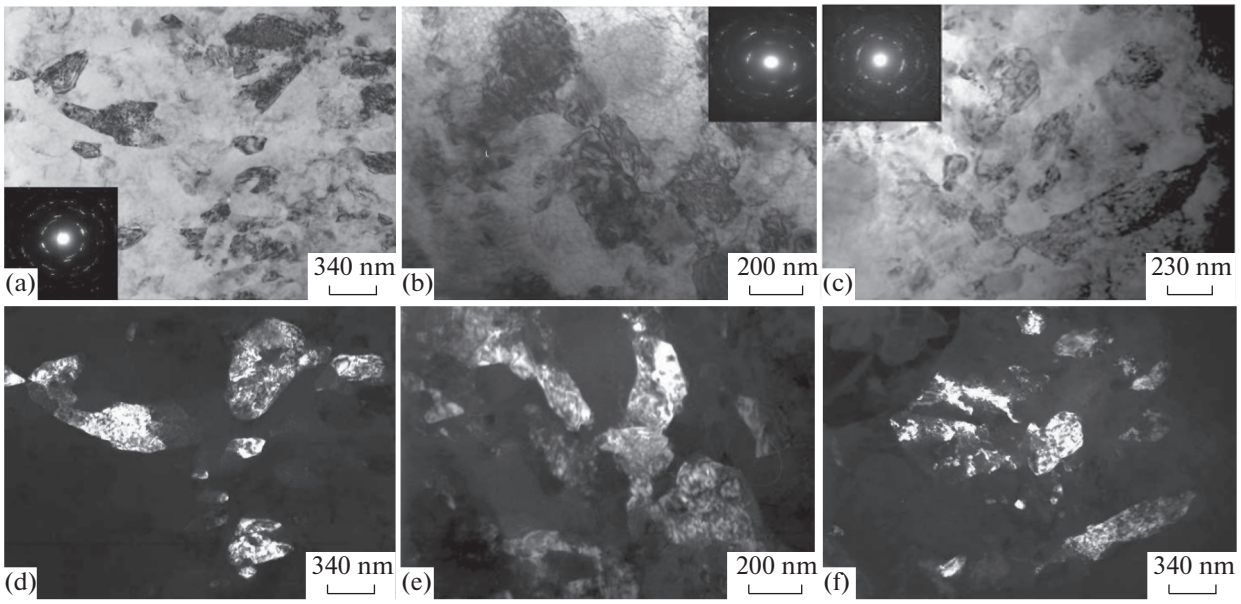

Fig. 5. Fine structure of the SMC alloy in various regions of the sample after shock compression. TEM: (a, b, c) bright-field images; (d, e, f) dark-field images; (a, d) near the loading surface; (b, e) fracture region; and (c, f) near the free surface.

2, $V = 250–300$ m/s) promotes the further growth of these characteristics. In this state, the Hugoniot elastic limit is maximum ($\sigma_{HEL} = 0.66$ GPa), which exceeds σ_{HEL} of the CG alloy by 78%. The dynamic yield stress is $\sigma_y = 0.31$ GPa, which is more than the yield stress of the CG alloy by 63%. The spall strength and the thickness of the spall plate are almost the same for all samples; i.e., a decrease in the size of fragments in the aluminum matrix does not affect the spall-fracture resistance of the alloy.

It was interesting to compare the dynamic characteristic of the SMC alloy formed by high-strain-rate plastic deformation (DCAP) with the corresponding characteristics of the SMC alloy of the same composition formed by ECAP. According to [23], the maximum value of the spall strength ($\sigma_{sp} = 0.9$ GPa) is obtained after four cycles of ECAP; in this case, we have $\sigma_{HEL} = 0.48$ GPa. The increase in σ_{HEL} as a result of the treatment of the alloy by ECAP was about 20%, and treatment by DCAP yields an increment of ~80% at the same crystallite size (400 nm) in SMC samples. An increase in the Hugoniot elastic limit to 0.72 GPa (comparable to σ_{HEL} of a sample after two DCAP passes) was only achieved by the complex combined treatment of samples, including warm and cold rolling after ECAP [23].

Thus, analyzing these results, we can note two points in the behavior of the DCAP SMS alloy under shock compression: an increase in the characteristics of elastic-plastic transition; and the retention of the spall strength on the level characteristic of the CG alloy.

Consider the structure of an SMC sample with a grain-subgrain structure retained after compression ($V = 250–300$ m/s, $N = 2$). Figure 5 shows (a, b, c) bright-field and (d, e, f) dark-field images of the retained samples obtained at the loading surface, near the spall surface, and at the free surface. If we compare the structure of these zones with the structure after DCAP (Fig. 1a, 1b), we see that the dynamic compression has a little effect on the morphological features of this structure. The ring-type diffraction pattern with azimuthal diffuse and spot reflections indicates the formation of a structure with low- and high-angle boundaries of fragments; i.e., a mixed nonequilibrium grain–subgrain structure with a size of fragments of about 400 nm is retained, as in the case after DCAP.

The difference of the fine structure in the regions located at different distances from the loading surface of the sample is mainly consists in the different numbers of structural defects, which is confirmed by the calculation of the dislocation density and microhardness (Table 2). The most work-hardened region is that located near the fracture surface, and the least-strengthened region is that located near the free surface.

Thus, under shock compression and DCAP, the main deformation mechanism is dislocation slip. In comparison with the structural state before shock compression (after DCAP), an increase in the dislocation density and in the microhardness is observed after shock compression, and the retention of the crystallite sizes in the same submicron range, which explains the high elastic-plastic and strength characteristics.

Table 2. Microhardness and dislocation density in various regions of an SMC sample before and after shock compression

Structure	H_V, MPa	ρ_d, $1/m^2$
SMC structure before shock compression	1200	1.0×10^{14}
SMC structure after shock compression near the loading surface	1400	1.8×10^{14}
SMC structure after shock compression in the fracture region	1400	2.2×10^{14}
SMC structure after shock compression near the free surface	1300	1.3×10^{14}

CONCLUSIONS

The experiments on the shock compression of an aluminum A5083 alloy have shown that the characteristics of the elastic-plastic transition (Hugoniot elastic limit, dynamic yield stress) of the SMC alloy produced by DCAP are higher than those of the CG analog by 78% and 63%, respectively. It has been established that the size of the structural elements and the type of the SMC structure formed upon DCAP influence the Hugoniot elastic limit. The maximum value (σ_{HEL} = 0.66 GPa) is achieved upon the formation of a mixed SMC structure with an average crystallite size of 400 nm. The measured critical breaking stresses during spall σ_{sp} of the tested alloy in the submicrosecond range of loading weakly depend on the initial structure and are approximately 1.5 GPa. The main deformation mechanism under shock compression is dislocation slip. According to TEM and XRD, the number of dislocations in the material increases as it approaches the region of the fracture surface and decreases near the free surface of the sample.

ACKNOWLEDGMENTS

The work was performed under the state assignment (theme "Structure", no. 01201463331) and was supported in part by the Russian Foundation for Basic Research (project no. 15-02-03225) and by the Presidium of the Russian Academy of Sciences (project no. 11P "Thermophysics of High Density Energy, Matter under High Pressure, Fundamental Problems of Plasma Confinement and Heating in Magnetic Traps"). The authors thank E. V. Shorokhov for conducting the experiments on dynamic channel-angle pressing and the administration of the UrFU for access to the scientific equipment of the URFU, supported by program 211 of the Government of the Russian Federation (agreement no. 02.A03.21.0006). The electron-microscopic studies were performed at the Center of Collaborative Access "Testing Center of Nanotechnology and Advanced Materials, Institute of Metal Physics, Ural Branch, Russian Academy of Science.

REFERENCES

1. G. V. Garkushin, G. E. Ivanchikhina, S. V. Razorenov, O. N. Ignatova, I. I. Kaganova, A.N. Malyshev, A. M. Podurets, V. A. Rayevskii, V. I. Skokov, and O. A. Tyupanova, "Mechanical properties of grade M1 copper before and after shock compression in a wide range of loading duration," Phys. Met. Metallogr. **111**, 197–206 (2011).
2. G. V. Garkushin, S. V. Razorenov, and G. I. Kanel, "Effect of structural factors on submicrosecond strength of D16T aluminum alloy," Tech. Phys. **53**, 1441–1446 (2008).
3. M. V. Aniskin, O. N. Ignatova, I. I. Kaganova, A. V. Kalmanov, E. V. Koshatova, A. I. Lebedev, V. V. Losev, A. M. Podurets, L. V. Polyakov, M. I. Tkachenko, A. N. Tsibikov, G. A. Salischev, G. V. Garkushin, S. V. Razorenov, and M. A. Zocher, "Mechanical properties of tantalum with different types of microstructure under high-rate deformation," Phys. Mesomech. **14**, 79–84 (2011).
4. S. V. Razorenov, G. V. Garkushin, G. I. Kanel', and O. N. Ignatova, "Resistance to dynamic deformation and fracture of tantalum with different grain and defect structure," Phys. Solid State **54**, 790–797 (2012).
5. S. V. Razorenov, G. I. Kanel, and V. E. Fortov, "Submicrosecond strength of aluminum and an aluminum–magnesium alloy AMg_6M at normal and enhanced temperatures," Phys. Met. Metallogr. **95**, 86–91 (2003).
6. G. I. Kanel, S. V. Razorenov, A. S. Savinykh, E. B. Zaretskii, and Yu. R. Kolobov, "Study of Structural Levels that Determine the Resistance to High-Strain-Rate Deformation and Fracture of Metals and Alloys," Preprint OVT, Russian Academy of Sciences, No. 1-478, Moscow, 2004.
7. G. V. Garkushin, O. N. Ignatova, G. I. Kanel, L. W. Meyer, and S. V. Razorenov, "Submicrosecond strength of ultrafine-grained materials," Mech.Solids **45**, 624–632 (2010).
8. R. Z. Valiev, Y. Estrin, Z. Horita, T. G. Langdon, M. J. Zehetbauer, and Y. T. Zhu, "Fundamentals of superior properties in bulk nanoSPD materials," Mater. Res. Lett. **4**, 1–21 (2016).
9. I. G. Brodova, A. N. Petrova, I. G. Shirinkina, E. V. Shorokhov, I. V. Minaev, I. N. Zhgilev, and A. V. Abramov, "Fragmentation of the structure in Al-based alloys upon high speed effect," Rev. Adv. Mater. Sci. **25**, 128–135 (2010).
10. I. G. Brodova, A. N. Petrova, and I. G. Shirinkina, "Comparing specific features of the structural formation of aluminum alloys during severe and intense plastic deformation," Tech. Phys. **76**, 1233–1237 (2012).
11. I. G. Shirinkina, A. N. Petrova, I. G. Brodova, V. P. Pilyugin, and O. A. Antonova, "Phase and struc-

tural transformations in the aluminum AMTs alloy upon severe plastic deformation using various techniques," Phys. Met. Metallogr. **113**, 170–175 (2012).

12. I. G. Brodova, I. G. Shirinkina, A. N. Petrova, O. V. Antonova, and V. P. Pilyugin, "Evolution of the structure of V95 aluminum alloy upon high-pressure torsion," Phys. Met. Metallogr. **111**, 630–638 (2011).
13. I. G. Brodova, I. G. Shirinkina, A. N. Petrova, V. P. Pilyugin, and T. P. Tolmachev, "Structure of an AMTs aluminum alloy after high-pressure torsion in liquid nitrogen," Phys. Met. Metallogr. **114**, 667–671 (2013).
14. I. G. Brodova, A. N. Petrova, S. V. Razorenov, and E. V. Shorokhov, "Resistance of submicrocrystalline aluminum alloys to high-rate deformation and fracture after dynamic channel angular pressing," Phys. Met. Metallogr. **116**, 519–526 (2015).
15. Z. Zhao, L. Wang, D. Fan, B. X. Bie, X. M. Zhou, T. Sou, Y. L. Li, M. W. Chen, C. L. Liu, M. L. Qi, M. H. Zhu, and S. N. Luo, "Macrodeformation twins in single-crystal aluminum," Phys. Rev. Lett. **116**, 075501 (2016).
16. E. V. Shorokhov, I. N. Zhgilev, and R. Z. Valiev, "Method of Material Dynamic Treatment," RF Patent 2283717, *Byull. Izobr.,* 2006, no. 26.
17. A. N. Petrova, I. G. Brodova, and E. V. Shorokhov, "Structural refinement in Al–Mg–Mn alloy by the dynamic channel angular pressing method," Perspekt. Mater. no. 12, 72–78 (2015).
18. I. G. Brodova, A. N. Petrova, S. V. Razorenov, O. P. Plekhov, and E. V. Shorokhov, "Deformation behavior of submicrocrystalline aluminum alloys during dynamic loading," Russ. Metall. (Metally) **2016**, 342–348 (2016).
19. T. Antoun, L. Seaman, D. R. Curran, G. I. Kanel, S. V. Razorenov, and A. V. Utkin, *Spall Fracture* 1 (Springer, Berlin, 2000).
20. L. M. Barker and R. E. Hollenbach, "Laser interferometry for measuring high velocities of any reflecting surface," J. Appl. Phys. **43**, 4669–4675 (1972).
21. S. P. Marsh, *LASL Shock Hugoniot Data* (Univ. California Press, Berkeley, 1980).
22. G. I. Kanel', S. V. Razorenov, A. V. Utkin, and V. E. Fortov, *Shock-wave Effects in Condensed Media* (Yanus-K, Moscow, 1996) [in Russian].
23. R. L. Whelchel, N. N. Thadhani, R. H. Sanders, L. J. Kecskes, and C. L. Williams, "Spall properties of 1 Al5083 plate fabricated using equi-channel angular pressing (ECAP) and rolling," J. Phys.: Conf. Ser. **500**, 112006 (2014). doi 10.1088/1742-6596/500/11/112066

Translated by G. Salnikov

SPELL: 1. spall